Microfluidic generation of therapeutically relevant polycaprolactone (PCL) microparticles: computational and experimental approaches

Alejandro Forigua, Arash Dalili, Rebecca Kirsch, Stephanie M. Willerth & Katherine S. Elvira

2022

Microfluidic generation of therapeutically relevant polycaprolactone (PCL) microparticles: Computational and experimental approaches

Alejandro Forigua,[†,‡] Arash Dalili,[†,‡] Rebecca Kirsch,[¶,‡] Stephanie M. Willerth,[*,¶,§,‖,‡,⊥] and Katherine S. Elvira[*,†,‡]

†Department of Chemistry, University of Victoria, Victoria, BC V8W 2Y2, Canada.

‡Centre for Advanced Materials and Related Technology (CAMTEC), University of Victoria, Victoria, BC V8W 2Y2, Canada.

¶Department of Mechanical Engineering, University of Victoria, Victoria, BC V8W 2Y2, Canada.

§Department of Biomedical Engineering, University of Victoria, Victoria, BC V8W 2Y2, Canada.

‖Division of Medical Sciences, University of Victoria, Victoria, BC V8W 2Y2, Canada.

⊥School of Biomedical Engineering, University of British Columbia, Vancouver, BC V6T 1Z3, Canada.

E-mail: willerth@uvic.ca; kelvira@uvic.ca

Abstract

Drug releasing microparticles play an important role in drug delivery as they can be used for site specific delivery, as well as control over the release time of therapeutics.

The use of microfluidic technologies for the fabrication of these particles is of increasing interest since they provide enhanced control over microparticle size and size distribution, compared to bulk production methods. However, the use of microfluidic platforms in the production of drug releasing microparticles with therapeutically relevant cargo still requires optimization depending on their application, and the effect of the addition of cargo on the production process is still unexplored. Here we show the formation of therapeutically relevant (in terms of size and dose of cargo) polycaprolactone (PCL) microparticles using a microfluidic platform, and analysed the effect of the addition of cargo in the microparticle size and size distribution. This microfluidic platform was designed with the aid of computational fluid dynamic simulations, allowing us to construct a PDMS microfluidic device capable of making microparticles in the range of 15 and 35 μm with low coefficient of variation (CV) both with and without cargo by varying the flow rate ratios of the phases used during droplet generation. Our data show the effect of the addition of cargo on the droplet and microparticle sizes and monodispersity. Our fabrication method allows the formation of spherical microparticles, optimal for biomedical applications. In addition, our microfluidic platform is able to maintain the generation of monodisperse droplets (with an average size of 52.5 μm) over extended periods of time, suggesting its capacity to be used for scaled-up production of PCL microparticles. This microfluidic device presents a robust and reliable platform for the fabrication of PCL microparticles with cargo, which can potentially be loaded with other relevant therapeutic molecules with biomedical applications.

Keywords: Microparticles, Drug Release, Droplets, Polycaprolactone, Microfluidics.

Introduction

Drug releasing particles have been of increasing interest in biotechnology and medicine due to their ability to provide site and time specific delivery of therapeutic agents.[1] Intravenous injections, nebulizers and vaccines are some of the modes of delivery that employ drug releasing

particles as a delivery mechanism, hence the recent interest in developing bespoke particles as well as more time and yield efficient fabrication methods.[2] Drug releasing particles can be classified depending on their size into micro and nanoparticles, and their functionality is directly related to their chemical composition and size,[3] with microparticles being of particular interest in tissue engineering.[4] A large portion of the drug releasing particles used for therapeutic purposes are made from polymeric materials due to their stability, biocompatability and their favourable release mechanisms under biological conditions. Some of the most common synthetic polymers used for the fabrication of drug releasing particles are poly(lactic-co-glycolic acid) (PLGA), polylactide (PLA), polyethelene glycol (PEG) and polycaprolactone (PCL).[5] PCL in particular has been widely used in a variety of applications because it degrades under biological conditions through the cleavage of its ester links by hydrolysis.[6] The degradation profile of PCL follows a first order hydrolysis, which means that it provides a controlled release of its cargo over extended periods of time (2-3 years) when compared to other commonly used materials such as PLA and PLGA (up to 6 months).[7] Recently, micrometer sized PCL particles have been used for drug delivery in tissue engineering through the inclusion of microparticles in the growth media.[8–10]

The most common methods to fabricate PCL microparticles are batch (a single stirred tank, with no addition of reagents during the reaction) and semi-batch methods (a single stirred tank with addition of reagents at any time).[5] Batch and semi-batch methods have challenges in terms of particle size distribution, with standard deviations usually close to 50%.[5] Hence, these methods are often followed by extensive filtering processes to achieve the desired sizes. Microfluidic technologies have recently emerged as a method to make microparticles with a narrow size distribution.[5] Some pertinent examples include the fabrication of PCL/PLA Janus particles as drug carriers, as well as PCL/PGLA/PCL Rhodamine B-loaded fibrous scaffolds with drug releasing capabilities.[11,12] Microfluidic devices consist of a network of micrometer scale channels for the control of small volumes of fluids (between 10^{-9} and 10^{-18} L).[13] Usually, aqueous droplets are formed in a continuous inmiscible

phase.[5,14] The size of the droplets formed depends on the flow rate ratios between the different phases, the geometry of the droplet creation junction, as well as the surface properties of the microfluidic devices. These parameters can be altered in *tandem* in a microfluidic device, to create bespoke droplets for particle formation.

Only a few examples exist showing the fabrication of PCL microparticles loaded with cargo using microfluidic technologies, since most focus on the production of nanoscale particles for quicker and more stable uptake of drugs in patients.[15] However, recent work has suggested that the more robust nature of micrometer sized particles allows higher dosages, which, since they cannot penetrate cell membranes, causes a slower release of cargo for long term therapies.[4,15] Most microfluidic methods for the formation of PCL based microparticles use multiple emulsions (such as oil-in-water-in-oil droplets), which usually involves increased complexity in the design of the microfluidic platform.[16] One example shows the introduction of chlorophyll into PCL microparticles for use as a food coloring agent with sizes ranging between 65 to 250 μm and standard deviations below 10%.[17] These PCL loaded microparticles showed improvement of the controlled release profile of chlorophyll, over a 25 hr release experiment, by lowering its degradation rate by a factor of 10. Another example used glass microcapillaries for the fabrication of PCL microparticles as transporters of bovine serum albumin (BSA), with sizes in the range of 25 to 47 μm and standard deviations of 25%.[18] Janus PLA/PCL microparticles can also be made using a double emulsion microcapillary microfluidic platform.[19] These particles had sizes in the range of 25 μm, however no standard deviation was reported. The Janus microparticles were loaded with a mixture of rhodamine and nile red. Using fluorescence microscopy the authors were able to determine that rhodamine has a preference for PLA and nile red for PCL, and they were hence able to make particles with more than one cargo and selective release profiles using a mixture of materials. Another example of the fabrication of Janus PLGA/PCL particles includes the use of a flow focusing microfluidic device, with microparticle sizes ranging from 25 to 50 μm, These microparticles have different degradation patterns to enable controllable release, such

as site specific and prolonged release.[20] Although most of these microfluidic platforms have successfully been able to fabricate the particles of interest, there is still work to be done in three areas, as we discuss in our recent review of these microfluidic technologies for the creation of drug releasing particles.[5] Firstly, there is a need for more methods to encapsulate cargo with relevant applications in areas such as medical therapeutics, nutritional and food science, industrial additives, etc. Secondly, we need to be able to fabricate microfluidic platforms with simpler designs and materials for non-skilled users. And lastly, we need microfluidic platforms capable of continuous production of large quantities of particles for scaled-up production.

Here we present a microfluidic platform capable of creating PCL microparticles with controlled particle sizes between 15 and 35 μm. We have evaluated the system numerically using computational fluid dynamics, and use polydymethylsiloxane (PDMS) as the device material. This developed platform is capable of producing PCL microparticles with no cargo and with therapeutically relevant cargo (guggulsterone, a hormone that has shown effectiveness in the differentiation of stem cells into neurons for the treatment of Parkinson's disease[8]), and we show that the long-term use of the microfluidic platform has no effect on particle morphology over time. The cargo was chosen based on our prior work because we needed a way to make microparticles with a narrower size distribution.[8] The microparticles produced on our microfluidic platform show comparable drug loading efficiency (49%) to those made in batch methods. Our platform shows promising results in terms of up-scaling production of the microparticles.

Results and discussion

Fluid dynamics simulations

Figure 1 shows a schematic of the microfluidic platform for the production of oil-in-water (o/w) droplets, which were then collected off-chip for solvent extraction and microparticle

formation. The microfluidic device used a flow-focusing geometry for droplet generation, as our prior analysis of the literature suggested this geometry was best suited for consistent droplet formation. A microfluidic device design feasibility study was performed using fluid dynamic simulations to determine the viability of the channel dimensions proposed for this device. The simulation results yielded a rapid assessment of the droplet generation geometry, the droplet generation regime and the starting flow rates needed for droplet formation.

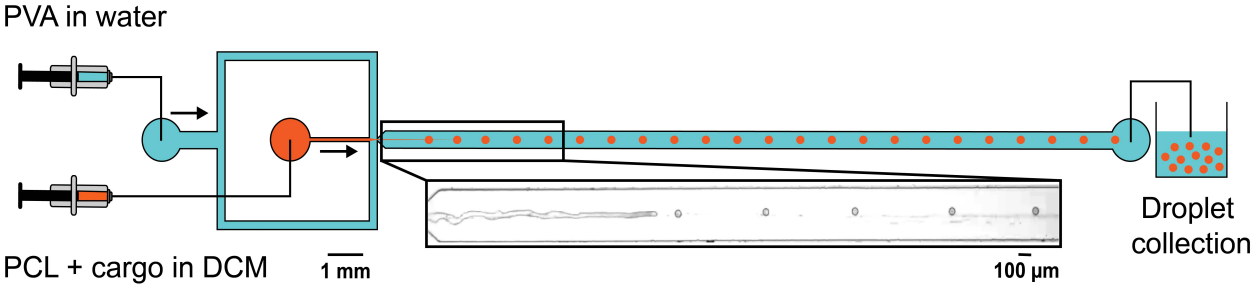

Figure 1: **Overview of the microfluidic platform.** Design of the microfluidic platform including the syringes for fluid insertion (not to scale), vial for droplet collection (not to scale) and composition of the phases being injected into the platform. Blue denotes the aqueous (continuous) phase (polyvinyl alcohol (PVA) solution in water) and orange denotes the droplet phase (polycaprolatone (PCL) in dichloromethane (DCM)), which can be dosed with cargo. These two phases meet at a flow focusing junction at which, at high flow rate ratios of the oil-to-aqueous phases, droplets form. The long channel immediately after the junction allows the formation of a jetting regime for droplet formation due to the high shear stress. The oil-in-water droplets are collected in a vial filled with PVA. By repeated inversion of the vial a spontaneous reduction of the viscosity of the oil-in-water system allows the precipitation of the solid microparticles.[21] The inset shows an image of the microfluidic device in operation, where oil-in-water droplets are formed in a jetting regime.

We simulated the 2-dimensional (2D) droplet generation process at a flow-focusing geometry, using COMSOL Multiphysics, with the aim of determining the feasibility of the droplet generator and the best flow rate ratio for droplet formation. The device geometry and the parameters used for the simulation are shown in Figure 2A. The literature states that to make small droplets the width of the aqueous inlet should be larger than that of the oil inlet, that the orifice angle should be 45°and that the chamber width should be larger than the widths of the inlets (Figure 2).[5] Hence our proposed design had a length and width of the main channel of 1.4 mm and 400 µm, respectively. The width of the aqueous (con-

tinuous) and dispersed (of which droplets are formed) phase inlets are 100 μm and 200 μm, respectively. The width and angle of the pinched section are 100 μm and 45°, respectively. The continuous phase flows from the top and bottom inlets (labelled as "aqueous"), the dispersed phase flows from the left inlet (labelled "oil solution"), and the outlet is on the right. The interface denotes the initial position of the continuous and dispersed phases. At the start of the simulation, all channels on the left of the interface are filled with continuous phase and those on the right are filled with the dispersed phase. The physical properties of the continuous and dispersed phases are shown in Table 1. The boundary conditions for the inlets, outlet, and walls were set to constant velocity, ambient pressure, and wetted wall, respectively. The contact angle of both phases were experimentally measured in the microfluidic channels, and found to be 0.52 radian.

Table 1: Fluid parameters for the dispersed phase (PCL in DCM) and the aqueous phase (PVA in water) used for the simulation of droplet generation.

Phases	**Density (kg/m^3)**	**Viscosity (mPa·s)**	**Interfacial tension (mN/m)**
PCL in DCM (3.3% w/v)	1330[22]	3.5[22]	4.0[22]
PVA in water (1% w/v)	1000[22]	1.2[22]	

The level-set method in the laminar two-phase flow package of COMSOL Multiphysics was used to model droplet generation in our microfluidic device. The governing equations consist of the continuity equation (Eq. 1) and the incompressible Navier-Stokes equation (Eq. 2), where ρ, μ, $\boldsymbol{u}$, p and F_{st} represent density, dynamic viscosity, velocity, pressure, and the surface tension force, respectively:

$$\nabla \cdot \boldsymbol{u} = 0 \tag{1}$$

$$\rho \frac{\partial \boldsymbol{u}}{\partial t} + \rho(\boldsymbol{u} \cdot \nabla)\boldsymbol{u} = \nabla[-pI + \mu(\nabla \boldsymbol{u} + \nabla \boldsymbol{u}^{\mathbf{2}})] + F_{st} \tag{2}$$

The interface position can be tracked by solving the level-set equation:

$$\frac{\partial \phi}{\partial t} + \boldsymbol{u} \cdot \nabla \phi = \gamma \nabla \cdot \left(-\phi \left(1 - \phi\right) \frac{\nabla \phi}{|\nabla \phi|} + \varepsilon \nabla \phi \right) \tag{3}$$

Where ϕ is the level-set function, and γ and ε are the re-initialization and interface thickness parameters, respectively. The terms on the left hand side of this equation describe the motion of the interface, while those on the right stabilize the numerical solution. ε controls the thickness of the interface and is set to the largest mesh size. The amount of stabilization of the level-set function is determined by the re-initialization factor, which is set to the maximum magnitude of the velocity of the fluid. The level-set function is set to 0 for the continuous phase and 1 for the dispersed phase, which means 0.5 is associated with the interface of the two phases.

The density and viscosity of the fluids are defined using the level-set function by equations 4 and 5, where subscripts 1 and 2 represent the continuous and dispersed phases, respectively:

$$\rho = \rho_1 + \left(\rho_2 - \rho_1\right) \phi \tag{4}$$

$$\mu = \mu_1 + \left(\mu_2 - \mu_1\right) \phi \tag{5}$$

After solving the continuity (Eq. 1), Navier-Stokes (Eq. 2), and level-set (Eq. 3), the pressure field, the velocity field, and the volume fraction of the continuous and dispersed phases were obtained, as shown in Figure 2B-F. This figure shows the simulated volume fraction profiles at velocity ratios of the continuous over the dispersed phase ranging from 20 to 50 on a 0 to 1 scale, where 0 (dark blue) indicates no presence of dispersed phase and 1 (dark red) indicates entirely dispersed phase. Our simulations show that at low velocity ratios, the shear stress on the oil solution is not high enough to break the solution and form droplets. As the velocity ratios go higher than 20, breaking up of the oil solution occurs and droplets form. Since the capillary number is relatively large (Ca ~1), the droplets were

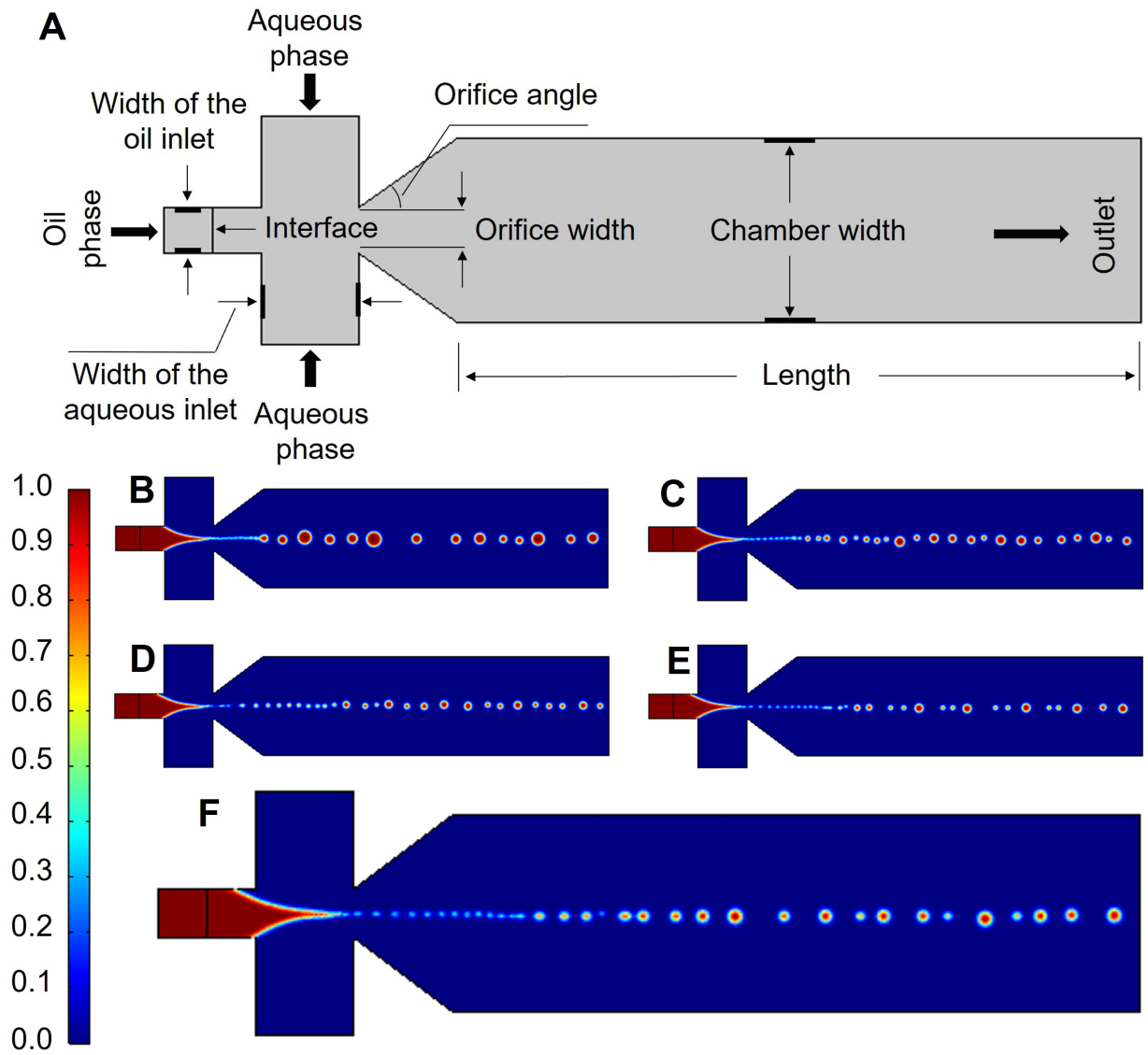

Figure 2: **Parameters for the computational fluid dynamics model. A**) Schematic of the geometry of the device that was used for the COMSOL Multiphysics model. The oil phase consisted of 3.3% w/v PCL in DCM and the aqueous phase consisted of 1% w/v PVA in water. The width of the oil and aqueous inlets were 100 μm and 200 μm, respectively. The orifice angle was 45° and the orifice width was 80 μm. The chamber was 1.4 mm long and 400 μm wide. **B-F)** Simulation of droplet formation at velocity ratios of 20, 25, 35, 40 and 50, respectively, of the oil and aqueous solutions as a colour scale from 0.0 (blue) to 1.0 (red), where 1 denotes the oil phase and 0 denotes the aqueous phase.

formed in a jetting regime, which is consistent with the literature.[23] The incremental increase of the velocity ratio from 20 to 50 consistently led to the formation of smaller droplets due to the higher shear stress on the droplets, leading to an average size of 43 $\pm$ 5 μm at the highest tested ratio (Figure 2F).

A mesh study was conducted for a velocity ratio to examine the influence of lattice resolution on the mean diameter of the generated droplets, and the data are presented in Figure S1 in the Supporting Information (SI). These results show minor differences between the last two mesh sizes. Therefore, considering the computational costs, a total number of elements of 43,561 were used for the numerical studies. Additionally, the accuracy of the COMSOL Multiphysics model was validated by comparing the simulation results with experimental data for the generation of de-ionized water droplets in silicon oil.[24] The results (Figure S2) show that the difference is below 7.1%, which validates the COMSOL Multiphysics model.

These simulations showed that the proposed microfluidic device design is suitable for droplet formation for the production of PCL microparticles. As is common in the field, the simulations do not account for the 3-dimensionality of experimental droplet generation, and hence the velocity rates cannot be directly translated to experimental flow rates due to the complex cross-sectional area of a jetting regime.[25] Therefore we used these velocity ratios as the starting point for the experimental formation of PCL microparticles.

Microparticle production from oil-in-water droplets

A microfluidic platform was built with the same geometry and dimensions as tested computationally with the aim of creating PCL microparticles of tunable sizes. We were also interested in seeing the effect of adding cargo to the microparticle production. The microfluidic device used a flow-focusing droplet generator and was fabricated using soft lithography from PDMS. PDMS-based microfluidic devices are optimal for water-in-oil (w/o) droplet formation, due to the hydrophobic nature of PDMS.[26,27] As oil-in-water (o/w) droplets were required for the fabrication of PCL microparticles, a hydrophilic substrate and surface mod-

ification of the PDMS device were used to form droplets. In other words, the PDMS devices were bonded directly to a glass slide, and the channels were treated with a 2% PVA (w/v) solution.

The inset in Figure 1 as well as Video S1 in the SI show the droplet generator in operation. Initially, "no cargo" microparticles were created using only PCL dissolved in DCM as the oil phase. Then "with cargo" microparticles were created by adding guggulsterone dissolved in ethanol to the oil phase to create microparticles with a concentration of 6 μg/mg (w/w, cargo/PCL). For both types of microparticles, the aqueous phase was 2% PVA (w/v) in water. Droplet formation was achieved at a 100:1 μL/min (aqueous:oil) flow rate ratio. Droplets formed consistently in a jetting regime, showing no coalescence in the collection vial. This verifies that our microfluidic platform was capable of generating droplets, translating into PCL microparticles after solvent extraction.

Figure 3 shows the size distribution of droplets (on-chip) and the microparticles (off-chip) formed after solvent extraction over a range of flow rates (100:1, 200:1, 300:1 and 350:0.5 μL/min) with no cargo (Figure 3A-D) and with cargo (Figure 3E-H). By doubling and then tripling the flow rate of the outer (water) phase we were able to study the effect of flow on droplet and microparticle size distribution. The final flow rates tested in both cases denotes a 7-fold increase in the flow rate ration and allowed us to determine the lowest droplet size possible with this microfliudic device design. Table 2 summarizes the distribution in droplet and microparticle size achieved at each flow rate ratio.

Figure 4 quantifies how the increase in the flow rate ratio affects the size of the droplets and particles. As expected, the higher the flow rate ratio, the smaller the droplet size, a trend which is less pronounced, but significant (i.e. $p<0.05$), in the size of the microparticles that are formed from these droplets. We also note that the variation in the droplet sizes is very small at all flow rate ratios, but larger for the microparticles. This suggests that it is the process of solidification that is introducing variation in the size, and presents an opportunity for future work in adjusting this process to enable even more monodisperse

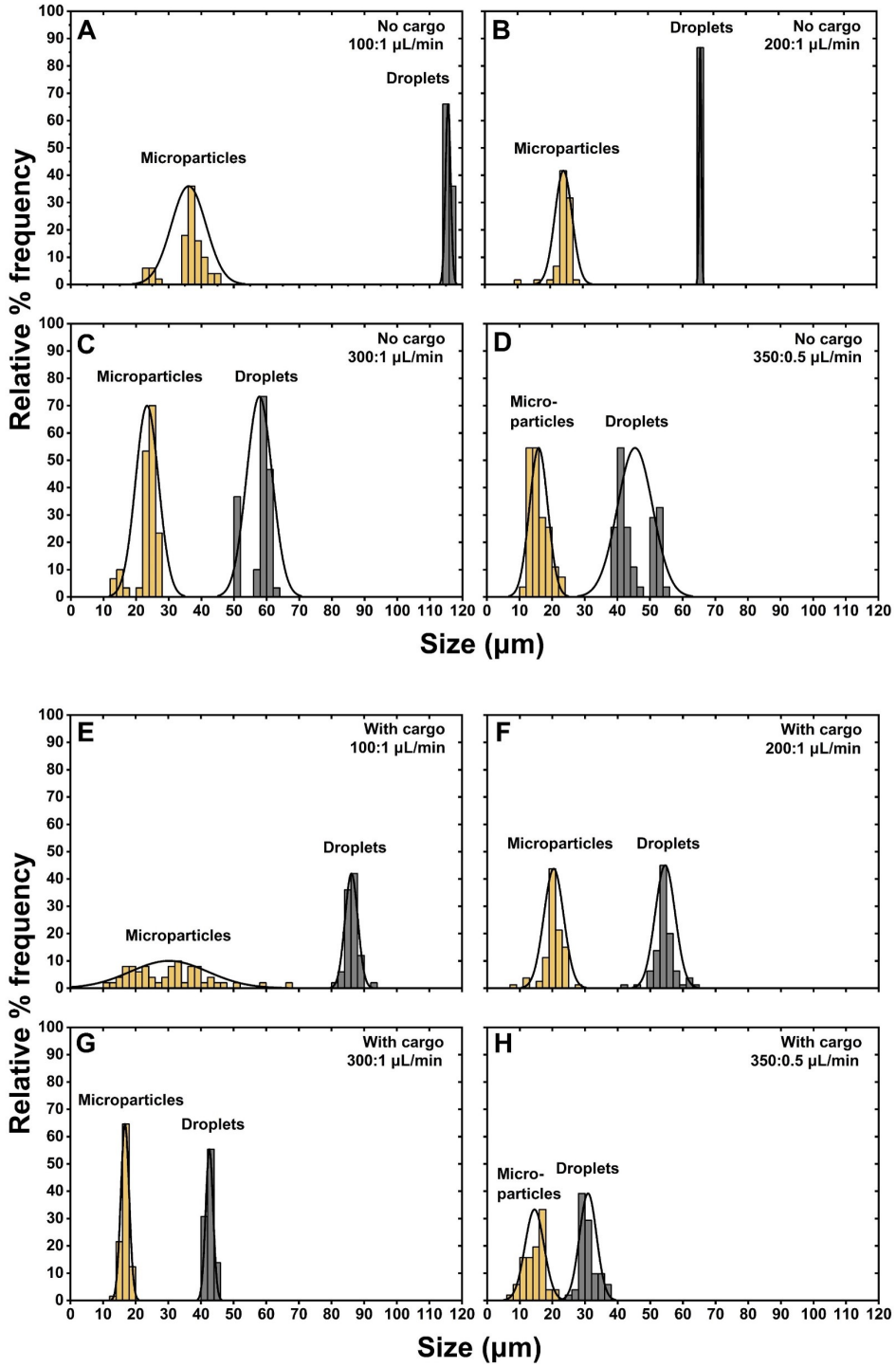

Figure 3: **Comparison of on-chip droplet size with off-chip microparticle size.** Histograms showing the relative percent frequency versus size and the fitted normal distribution of droplets measured on-chip using the Droplet morphometry and velocimetry software (DMV) (yellow data) and PCL microparticles measured off-chip after solvent extraction using scanning electron microscopy (SEM) (grey data) formed at aqueous to oil flow rates of 100:1 µL/min, 200:1 µL/min, 300:1 µL/min and 350:0.5 µL/min for **A-B)** microparticles with no cargo, and **E-H)** for microparticles with cargo. N = 50, over an average of 3 runs for each data set. The average size, standard deviation and coefficient of variation are reported for each data set in Table 2. Statistical analysis was performed using OriginPro 2018

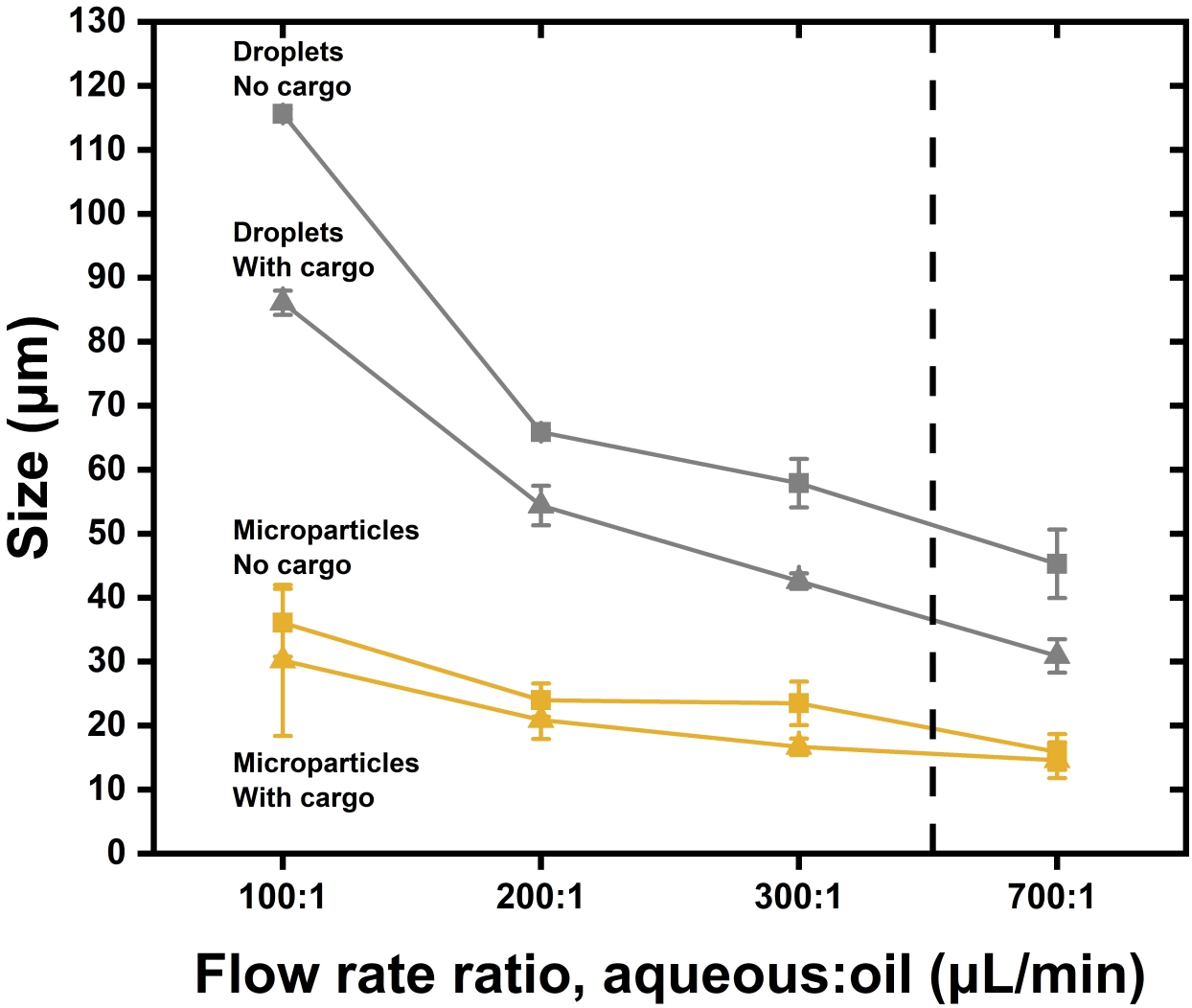

Figure 4: **Quantifying the effect of flow rate on droplet and microparticle sizes.** Average droplet (grey data) and microparticle sizes (yellow data) with (triangles) and without cargo (squares) are plotted as a function of aqueous to oil flow rate ratios. The error bar represents the standard deviation of each measurement. Lines between data values are plotted to aid visualisation. The vertical dashed line highlights the point at which the flow rate ratio increase is not linear.

Table 2: Summary of average size of droplets and microparticles at flow rate ratios between the aqueous and oil phases of 100:1, 200:1, 300:1, 350:0.5 μL/min. %CV is defined as the ratio of the standard deviation (SD) over the average size.

	Flow rate ratio (μL/min)	Droplets			Microparticles		
		Average size (μm)	SD (μm)	%CV	Average size (μm)	SD (μm)	%CV
No cargo	100:1	115.6	0.8	0.7	36.1	5.3	14.7
	200:1	65.9	0.3	0.5	24.0	2.6	11.0
	300:1	57.9	3.8	6.5	23.5	3.4	14.4
	350:0.5	45.3	5.3	11.8	15.9	2.8	17.6
With cargo	100:1	86.1	1.9	2.3	30.2	11.8	39.0
	200:1	54.4	3.1	5.8	20.9	3.0	14.2
	300:1	42.6	1.2	2.8	16.7	1.3	8.0
	350:0.5	30.9	2.6	8.5	14.6	2.8	19.5

microparticles to be produced. Overall, the addition of cargo decreases the droplet and microparticle size for each flow rate ratio, yet this effect is still significant but less pronounced for the microparticles. It has been shown previously that the addition of cargo can affect microparticle size when these are fabricated using a droplet generator.[19] This suggests that the addition of guggulsterone dissolved in ethanol changes the fluid parameters of the aqueous phase sufficiently to affect droplet formation - causing a shrinking trend in the microparticles after precipitation, and provides valuable information regarding the importance of developing methods for microparticle formation that include all required components.

Characterization of microparticle encapsulation efficiency

The encapsulation efficiency of the microparticles was determined using a fluorescent probe inserted at the same concentration as the guggulsterone and measured using fluorimetry (see SI Figure S3 for calibration curve), showing the encapsulation efficiency of 49% ± 4%, which is comparable to batch methods that make PCL microparticles with similar sizes.[8] Figure 5 shows the scanning electron microscopy (SEM) images of the microparticles after solvent extraction. The figure shows microparticles formed from droplets created at flow rate ratios of 100:1 μL/min, 200:1 μL/min, 300:1 μL/min and 350:0.5 μL/min for microparticles with no cargo (A-D) and with cargo (E to F) respectively. The images show the defined spherical shape of the microparticles. Since the aim is for these particles to be used for drug delivery,

a spherical structure is ideal due to its release pattern under biological conditions, as well as conferring rigidity in the scaffolding of the extracellular matrix for tissue engineering.[8,9,28,29] The SEM images show that a flow rate ratio of 300:1 μL/min (Figure 5C,G), gives the most defined spheres. However, as the SEM images only show a sample of the entire population of microparticles, the statistical analysis discussed previously (Table 2) display a quantitative insight where microparticles with cargo are more monodisperse compared to those with no cargo.

Microfluidic device performance over time

Scaling-up the production of microparticles is key for the use of microfluidic technologies outside of academic laboratories, and yet the performance of microfluidic devices over time is rarely characterised. Figure 6 shows the quantification of the variation in the size of droplets with cargo created at a flow rate ratio of 300:1 μL/min over the course of 75 min. Our data show no significant difference between the average droplet sizes collected at 0 min and 15 min, and between the average droplet sizes collected between 30 and 75 min. The change in average droplet sizes from 48.1 ± 4.4 μm at 15 min to 51.8 ± 4.6 μm at 30 min, together with the stabilisation of the droplet sizes after 30 min of device operation, suggests that there is an initial equilibration period for the droplet generator. This stabilization period can be described as the transition from a Brownian (i.e. random) nucleation to laminar-shear induced (i.e. stable) nucleation after 30 min.[30] If the aim is to increase droplet monodispersity over time, these should be collected after 30 min of device operation. It is worth noting, however, that the data for the same flow rate shown in Figure 4 correspond to droplets collected over the course of 75 min, and they show a very small variation in droplet size. This suggests that our microfluidic platform performs well over time, and could therefore be used for the scaled-up production of therapeutically relevant drug releasing microparticles. Nonetheless, the production rate of a single microfluidic device can be increased by the parallelization of multiple droplet generators, and this has become more standard in the

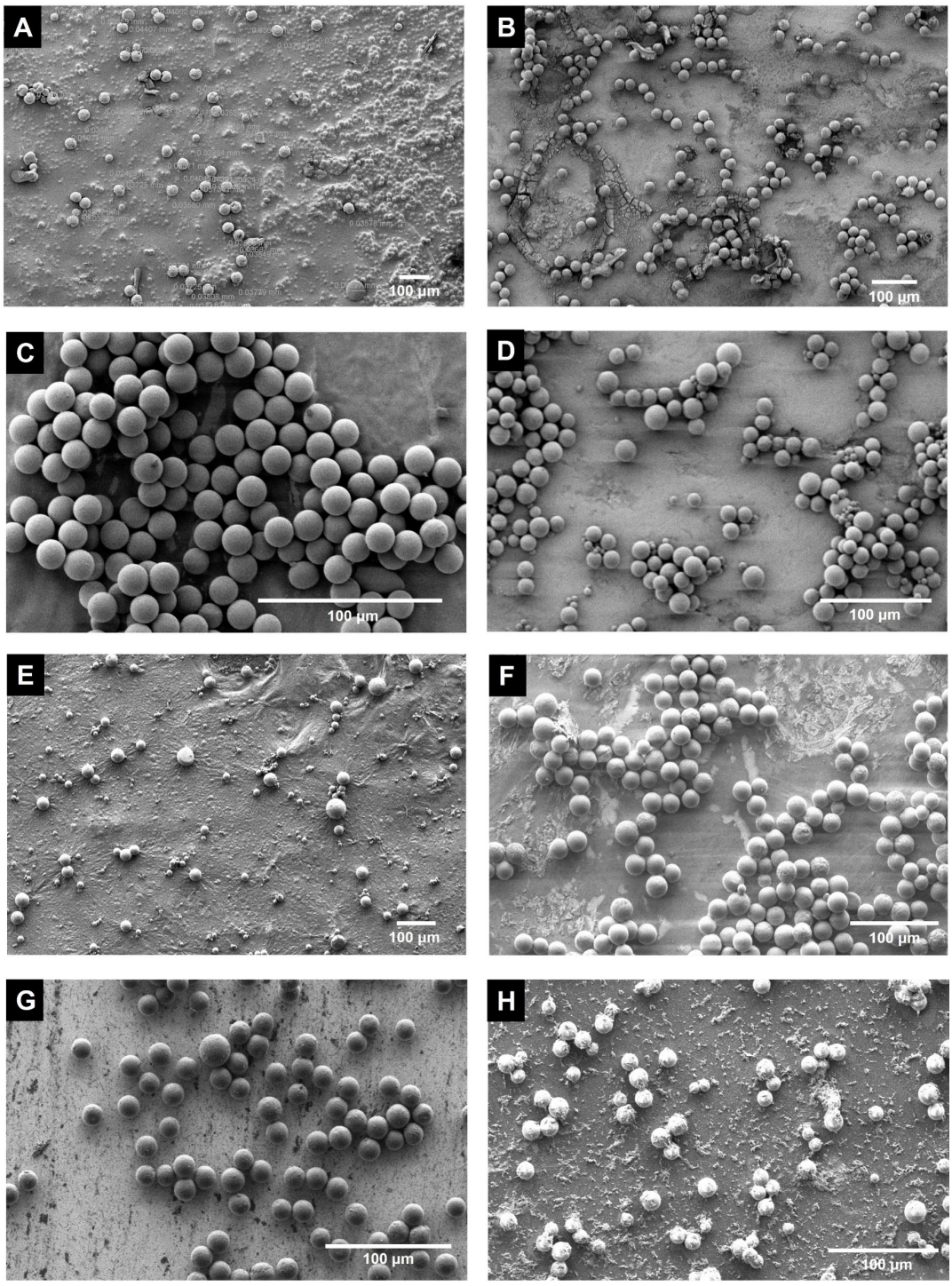

Figure 5: **SEM images of PCL microparticles.** PCL microparticles with no cargo formed at aqueous to oil flow rates of **A)** 100:1 µL/min, **B)** 200:1 µL/min, **C)** 300:1 µL/min and **D)** 350:0.5 µL/min; and microparticles with cargo formed at aqueous to oil flow rates of **E**) 100:1 µL/min, **F)** 200:1 µL/min, **G)** 300:1 µL/min and **H)** 350:0.5 µL/min.

generation of drug releasing particles in industry.[5] It is interesting to note that this is the case even when using solvents such as DCM and ethanol that are generally less compatible with PDMS.[26] However, PDMS devices can still present challenges in re-usability when compared to other materials used currently in industrial processes such as glass, silicon or ceramic, which are typically more robust and compatible with a variety of solvents.[5]

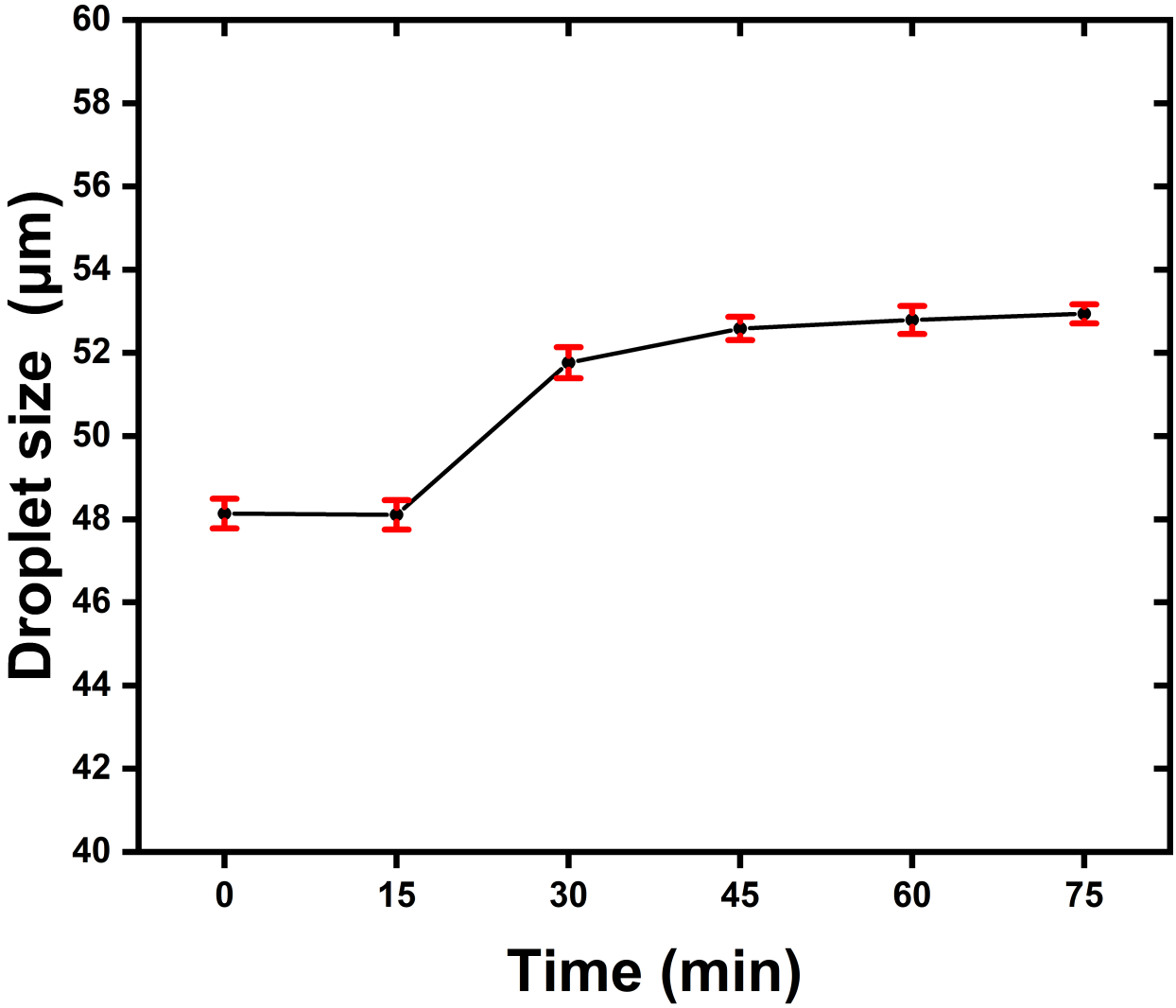

Figure 6: **Quantification of device performance over time.** Quantification of the variation in size of the droplets with cargo over time at an aqueous to oil flow rate of 300:1 µL/min. Average droplet sizes are plotted as a function of time. Error bars represent the standard error, with values of 0.4 µm for 0 to 30 min, 0.3 µm for 45 to 65 min, and 0.2 µm for 75 min. The lines between data values are plotted to aid visualisation. N = 150 (over an average of three runs).

Conclusions

We have designed and tested a microfluidic platform for the fabrication PCL microparticles with and without cargo, that is able to create them with low dispersity and sizes in the range of 15 and 35 μm by altering the flow rate ratios of the injected phases. This platform was designed based on initial data acquired from 2D fluid dynamic simulations, and fabricated from PDMS. The analysis of droplets and microparticle sizes and the comparison between the addition or not of cargo, allowed us to determine the effect of the addition of cargo on size and dispersity are dependant. The microparticles are spherical, as shown by SEM data, which is optimal for biological and medical applications, like drug delivery and tissue engineering. Finally, our PDMS microfluidic platform shows a good performance in droplet formation over extended periods of time, which demonstrates the potential of such a platform for scaled-up production. Future work will focus on further improving the dispersity in microparticle size, in reducing their overall size and including other therapeutically relevant cargos.

Materials and methods

Materials

Polydimethylsiloxane (PDMS, Dow Sylgard 184) was purchased from Ellsworth Adhesives. Poly(vinyl alcohol) (PVA, MW 13,000 - 23,000, 87-89% hydrolyzed), polycaprolactone (PCL, MW 70,000 - 90,000), fluorescein (free acid) and chlorotrimethylsilane (≥ 98%) were purchased from Sigma Aldrich. (Z)-Guggulsterone (≥ 98%) was purchased from StemCell Technologies. Absolute ethanol (≥ 99%) was purchased from Commercial Alcohols. Acetate masks were printed at 10 μm resolution by CAD/Art Services Inc. Silicon wafers (100 mm diameter) were purchased from Silicon Materials. SU-8 3050 and developer were purchased from MicroChem. Polytetrafluoroethylene (PTFE, 1/16" outer diameter, 750 μm inner diameter) tubing was purchased from Chromatographic Specialties Inc.

Computational method

Computational Fluid Dynamics simulations were performed using COMSOL Multiphysics (Version 5.6). The droplet generator was simulated as a 2-dimensional (2D) droplet generator, using the level-set method in the laminar two-phase package, solving numerically the continuity, Navier-Stokes, and level-set equations, to obtain the velocity and pressure field, as well as the volume fraction of the two-phase system.

Preparation of solutions

To prepare the aqueous phase (2% w/v PVA in water), 8 g of PVA in 400 mL deionized water were mixed at 85°C at 850 rpm until the PVA had dissolved and a clear solution was formed. To prepare the oil phase, 800 mg of PCL were dissolved into 15 mL of DCM at 900 rpm until a clear solution was formed. For the microparticles with cargo, the oil phase also contained 4.8 mg of cargo dissolved in 1 mL of ethanol, to create microparticles at a concentration of 6 μg/mg (w/w, cargo/PCL).

Fabrication of the microfluidic platform

The design of the microfluidic platform was created using AutoCAD, and printed on an acetate film to create a positive photomask. The master mould was fabricated by dehydrating a silicon wafer at 200°C for 18 h on a hotplate. A layer of SU-8 3050 negative photoresist (50 ± 2 μm) was then spin-coated onto the wafer, and soft baked (5 min at 35°C, 2 min at 65°C and 30 min 95°C). After baking, the wafer was exposed to UV light (365 nm, 11.0 s, 19.96 mW/cm^2) through the photomask, and subjected to a second soft bake. To remove non-crosslinked SU-8, the wafer was rinsed with developer, followed by isopropanol. The wafer was then exposed to UV light a second time (365 nm, 90 s, 19.96 mW/cm^2) and hard baked (30 min at 200°C) to ensure adhesion of the SU-8.

The wafer was placed in a desiccator with 50 μL chlorotrimethylsilane for 45 min, allowing

the silane to deposit on the surface, and then inserted into a 3D-printed holder and secured using two clamps. A 10:1 ratio of PDMS base and curing agent were mixed thoroughly and poured onto the mold. The mixture was degassed for 1 h under vacuum to remove air bubbles and the PDMS was cured in a preheated oven at 65°C overnight under ambient conditions. The cured PDMS was peeled from the mold, followed by cutting out the individual devices and punching the inlets and outlets using a 1 mm biopsy punch. Glass microscopy slides were used as the base for the devices. The PDMS devices and glass slides were thoroughly washed with soapy Milli-Q water and rinsed sequentially with Milli-Q water, isopropanol, ethanol and again with Milli-Q water; followed by blow drying using a filtered air gun and baking at 90°C for 30 min. The devices and glass slides were treated with air plasma (Diener Electronic, Zepto ONE, 60 s, 100 W, 0.60 mbar), and the activated surfaces were placed in contact with each other to allow bonding of the PDMS device to the glass substrate.

The microfluidic channels were treated in order to obtain a hydrophilic surface. The same 2% PVA solution used to make the microparticles was loaded into a 1 mL Hamilton glass gas-tight syringe. One of the inlets of the microfluidic device was attached to the syringe loaded with PVA and a piece of PTFE tubing was attached to the outlet. The other inlets in the device were plugged with pieces of sealed PTFE tubing. The PVA solution was manually flowed through the device for 10 min, ensuring that the solution filled all the channels inside the device. Filtered air was then pushed through the device. This was followed by baking the devices at 100°C for 15 min. Devices were kept at 65°C for at least 72 h prior to use.

Production of microparticles

All the experiments were visualised using a Nikon Eclipse Ti2-U inverted microscope and a Phantom VEO 710L high speed camera. Reagents were introduced into the microfluidic device using neMESYS syringe pumps (Cetoni, Germany), coupled to a 1 mL and a 25 mL Hamilton glass gas-tight syringe using three matched lengths of PTFE tubing. The 25 mL syringe was loaded with PVA solution (aqueous phase) and the 1 mL syringe was loaded with

PCL solution (oil phase). The aqueous phase was initially introduced at a flow rate of 50 µL/min for 1 min, flooding the channels with PVA and purging the system of air. Then the aqueous phase flow rate was increased to 100 µL/min and the oil phase was introduced at a flow rate of 1 µL/min, always checking that no oil phase was back-flowing into the aqueous phase inlets. Once a stable flow was reached and droplets were forming, the aqueous phase flow rate was increased by increments of 50 µL/min until the desired flow rate was achieved, and left to stabilize until droplets were formed consistently prior to data acquisition. The outlet tubing was placed in a glass vial filled with 2 mL of PVA solution to collect the droplets. To form the microparticles, the vial was capped, manually inverted repeatedly for 30 s and left at room temperature overnight in the dark to ensure the extraction of DCM.

Size measurements of droplets and microparticles

Droplets were measured on-chip using the video processing software Droplet morphometry and velocimetry (DMV).[31] This software uses an algorithm were a background image is subtracted from the original image. The edge of the droplets is detected by the increase in the contrast of the image, and then integration of the perimeter is performed to obtain the diameter of the droplet. Frame correlation is performed to avoid replicates of the same droplet being measured in subsequent frames. The internal channel width of the microfluidic device was used to set a scale for measuring droplets in the DMV software.

Microparticles were imaged and measured off-chip using scanning electron microscopy (SEM, Hitachi S-4800). The microparticles were first washed 7 times with deionized water (7 min at 3000 rpm for the first wash, then for 5 min at 3000 rpm for each remaining wash), then freeze-dried in a lyophilizer (VirTis Freezemobile 12EL-85°C FreezeDryer Lyophilizer w/16-Port Tree Manifold) for 24 h. Microparticles were stored at -80°C until analysis. For analysis, the microparticles were loaded onto an SEM stub and 50 µL of ethanol was used to evenly disperse them. The samples were sputter coated with gold-palladium (Anatech Hummer VI, Au/Pd) before imaging. While sputter coating the samples, plasma discharge

at a current of 10 mA was used for four minutes. Microparticle diameters were measured using the Quartz-PCL Image Management Systems software (Quartz Systems).

Quantification of cargo encapsulation

The encapsulation efficiency of the microparticles was measured using fluorescein as a fluorescent probe. The measurements were performed using a SpectraMax M5 plate reader in fluorescence mode. The excitation wavelength was 470 nm, and the measured emission wavelength was 540 nm. The reported cargo load value represents the replicate of 3 different experiments on different microfluidic devices. The SI provides details regarding the quantification of the fluorescein cargo.

Statistical analysis

Statistical analysis was performed using OriginPro 2018 data. The data for the effect of flow rate and the addition of cargo on droplet and microparticle size (shown in Figure 4) was analysed using a two-way ANOVA and Tukey's post-hoc analysis was used to assess the effect of the combination of both the size. The data for effect of time on droplet size (shown in Figure 6) was analysed using a one-way ANOVA and Tukey's post-hoc analysis was used to asses the significance of the difference in size at each time point. All statistical analyses were performe at a confidence level of 95% ($p>0.05$).

Acknowledgement

We acknowledge and respect the Lekwungen peoples on whose traditional territory the University of Victoria stands, and the Songhees, Esquimalt and WSÁNEĆ peoples whose historical relationships with the land continue to this day. Dr. Willerth receives funding from the Canada Research Chairs program, and the Canadian Institutes for Health Research. Dr. Elvira receives funding from the Canada Research Chairs program, and the Michael Smith

Foundation for Health Research Scholar program in partnership with the Pacific Alzheimer Research Foundation. This research was partially funded using Innovate BC's Ignite program.

Authors contributions

AF designed the microfluidic platform, acquired all experimental data except as detailed below, analysed all data and wrote the first draft of the manuscript. AD developed the COMSOL Multiphysics simulations and analysed all the numerical data. RLK made the oil phase solutions and acquired the SEM data. KSE reviewed and edited the manuscript, and supervised AF and AD. SW supervised RLK. All authors approved the final version of the manuscript.

Supporting Information Available

The following files are available free of charge.

- Graph for mesh sensitivity analysis.
- Graph for numerical model validation.
- Calibration curve for calculation of the loading of the microparticles.
- Video of droplet formation on the microfluidic device.

References

(1) Sung, Y. K.; Kim, S. W. Recent advances in polymeric drug delivery systems. *Biomaterials Research* **2020**, *24*, 12.

(2) Fenton, O. S.; Olafson, K. N.; Pillai, P. S.; Mitchell, M. J.; Langer, R. Advances in biomaterials for drug delivery. *Advanced Materials* **2018**, *30*, 1705328.

(3) Molavi, F.; Barzegar-Jalali, M.; Hamishehkar, H. Polyester based polymeric nano and microparticles for pharmaceutical purposes: A review on formulation approaches. *Journal of Controlled Release* **2020**, *320*, 265–282.

(4) Oliveira, M. B.; Mano, J. F. Polymer-based microparticles in tissue engineering and regenerative medicine. *Biotechnology Progress* **2011**, *27*, 897–912.

(5) Forigua, A.; Kirsch, R. L.; Willerth, S. M.; Elvira, K. S. Recent advances in the design of microfluidic technologies for the manufacture of drug releasing particles. *Journal of Controlled Release* **2021**, *333*, 258–268.

(6) Kumari, A.; Yadav, S. K.; Yadav, S. C. Biodegradable polymeric nanoparticles based drug delivery systems. *Colloids and Surfaces B: Biointerfaces* **2010**, *75*, 1–18.

(7) Kamaly, N.; Yameen, B.; Wu, J.; Farokhzad, O. C. Degradable controlled-release polymers and polymeric nanoparticles: Mechanisms of controlling drug release. *Chemical Reviews* **2016**, *116*, 2602–2663.

(8) Agbay, A.; Vega, L. D. L.; Nixon, G.; Willerth, S. Guggulsterone-releasing microspheres direct the differentiation of human induced pluripotent stem cells into neural phenotypes. *Biomedical Materials* **2018**, *13*, 034104.

(9) De la Vega, L.; Karmirian, K.; Willerth, S. M. Engineering neural tissue from human pluripotent stem cells using novel small molecule releasing microspheres. *Advanced Biosystems* **2018**, *2*, 1–11.

(10) Woodruff, M. A.; Hutmacher, D. W. The return of a forgotten polymer - polycaprolactone in the 21st century. *Progress in Polymer Science* **2010**, *35*, 1217–1256.

(11) Hakim, S. L.; Kusumasari, F. C.; Budianto, E. Optimization of biodegradable PLA/PCL microspheres preparation as controlled drug delivery carrier. *Materials Today: Proceedings* **2020**, *22*, 306–313.

(12) Milosevic, M.; Stojanovic, D. B.; Simic, V.; Grkovic, M.; Bjelovic, M.; Uskokovic, P. S.; Kojic, M. Preparation and modeling of three-layered PCL/PLGA/PCL fibrous scaffolds for prolonged drug release. *Scientific Reports* **2020**, *10*, 11126.

(13) Elvira, K. S.; Casadevall i Solvas, X.; Wootton, R. C. R.; deMello, A. J. The past, present and potential for microfluidic reactor technology in chemical synthesis. *Nature Chemistry* **2013**, *5*, 905–915.

(14) Glawdel, T.; Elbuken, C.; Ren, C. L. In *Encyclopedia of microfluidics and nanofluidics*; Li, D., Ed.; Springer US: Boston, MA, 2013; pp 1–12.

(15) García, M. C. *Engineering Drug Delivery Systems*; Elsevier, 2020; pp 71–110.

(16) Yaqoob Khan, A.; Talegaonkar, S.; Iqbal, Z.; Jalees Ahmed, F.; Krishan Khar, R. Multiple emulsions: An overview. *Current Drug Delivery* **2006**, *3*, 429–443.

(17) Hsiao, C.-J.; Lin, J.-F.; Wen, H.-Y.; Lin, Y.-M.; Yang, C.-H.; Huang, K.-S.; Shaw, J.-F. Enhancement of the stability of chlorophyll using chlorophyll-encapsulated polycaprolactone microparticles based on droplet microfluidics. *Food Chemistry* **2020**, *306*, 125300.

(18) Pessi, J.; Santos, H. A.; Miroshnyk, I.; Joukoyliruusi,; Weitz, D. A.; Mirza, S. Microfluidics-assisted engineering of polymeric microcapsules with high encapsulation efficiency for protein drug delivery. *International Journal of Pharmaceutics* **2014**, *472*, 82–87.

(19) Ekanem, E. E.; Nabavi, S. A.; Vladisavljević, G. T.; Gu, S. Structured biodegradable

polymeric microparticles for drug delivery produced using flow focusing glass microfluidic devices. *ACS Applied Materials & Interfaces* **2015**, *7*, 23132–23143.

(20) Li, W.; Dong, H.; Tang, G.; Ma, T.; Cao, X. Controllable microfluidic fabrication of Janus and microcapsule particles for drug delivery applications. *RSC Advances* **2015**, *5*, 23181–23188.

(21) Aravand, M. A.; Semsarzadeh, M. A. Particle formation by emulsion inversion method: Effect of the stirring speed on inversion and formation of spherical particles. *Macromolecular Symposia* **2008**, *274*, 141–147.

(22) Bile, J.; Bolzinger, M.-A.; Vigne, C.; Boyron, O.; Valour, J.-P.; Fessi, H.; Chevalier, Y. The parameters influencing the morphology of poly(E-caprolactone) microspheres and the resulting release of encapsulated drugs. *International Journal of Pharmaceutics* **2015**, *494*, 152–166.

(23) Sattari, A.; Hanafizadeh, P.; Hoorfar, M. Multiphase flow in microfluidics: From droplets and bubbles to the encapsulated structures. *Advances in Colloid and Interface Science* **2020**, *282*, 102208.

(24) Meng, X.; Yu, Y.; Jin, G. Numerical simulation and experimental verification of droplet generation in microfluidic digital PCR chip. *Micromachines* **2021**, *12*, 409.

(25) Kovalchuk, N. M.; Sagisaka, M.; Steponavicius, K.; Vigolo, D.; Simmons, M. J. H. Drop formation in microfluidic cross-junction: Jetting to dripping to jetting transition. *Microfluidics and Nanofluidics* **2019**, *23*, 103.

(26) Lee, J. N.; Park, C.; Whitesides, G. M. Solvent compatibility of poly(dimethylsiloxane)-based microfluidic devices. *Analytical Chemistry* **2003**, *75*, 6544–6554.

(27) Elvira, K. S.; Gielen, F.; Tsai, S. S. H.; Nightingale, A. M. Materials and methods for droplet microfluidic device fabrication. *Lab on a Chip* **2022**, *22*, 859–875.

(28) Dash, T. K.; Konkimalla, V. B. Poly-E-caprolactone based formulations for drug delivery and tissue engineering: A review. *Journal of Controlled Release* **2012**, *158*, 15–33.

(29) Dhandayuthapani, B.; Yoshida, Y.; Maekawa, T.; Kumar, D. S. Polymeric scaffolds in tissue engineering application: A review. *International Journal of Polymer Science* **2011**, *2011*, 1–19.

(30) Bal, V.; Bandyopadhyaya, R. Mechanistic aspects in the formation of nano- and submicron particles in a batch and a continuous microfluidic reactor: Experiment, modeling and simulation. *Chemical Engineering Journal* **2019**, *371*, 43–54.

(31) Basu, A. S. Droplet morphometry and velocimetry (DMV): A video processing software for time-resolved, label-free tracking of droplet parameters. *Lab on a Chip* **2013**, *13*, 1892.